Dense melt residues drive near-MOR 'hot-spots'

Jordan J.J. Phethean[1]*, Martha Papadopoulou[2], and Alexander L. Peace[3]

[1] School of Environmental Science, University of Derby, Kedleston Road, Derby, UK

[2] School of Geography, Geology and the Environment, University of Leicester, University Road, Leicester

[3] School of Earth, Environment and Society, McMaster University, Hamilton, Ontario, Canada

* j.phethean@derby.ac.uk

Keywords

Hot-spot; Mantle dynamics; Inverted convection; Melt residue density; Chemical depletion buoyancy

ABSTRACT

The geodynamic origin of melting anomalies found at the surface, often referred to as 'hot-spots', is classically attributed to the mantle plume. The distribution of 'hot-spots' along mid-ocean ridge spreading systems around the globe, however, questions the universal validity of this concept. Here, the preferential association of 'hot-spots' with slow- to intermediate-spreading centres and not fast-spreading centres, an observation contrary to the expected effect of ridge suction forces on upwelling mantle plumes, is explained by a new mechanism for producing melting anomalies at shallow (< 2.3 GPa) depths. By combining the effects of both chemical and thermal density changes during partial melting of the mantle (using appropriate latent heat and depth dependant and thermal expansivity

parameters) we find that mantle residues experience an overall instantaneous increase in density when melting occurs at < 2.3 GPa. This controversial finding is due to thermal contraction of material during melting, which at shallow pressures (where thermal expansivities are highest), outweighs the chemical buoyancy due to melting. These dense mantle residues are likely to locally sink beneath spreading centres if ridge suction forces are modest, thus driving an increase in the flow of fertile mantle through the melting window and increasing magmatic production. This leads us to question our understanding of sub-spreading centre dynamics, where we now suggest a portion of locally inverted mantle flow results in 'hot-spots'. Such inverted flow presents an alternative mechanism to upwelling hot mantle plumes for the generation of excess melt at near-ridge 'hot-spots', i.e. dense downwellings of mantle residue. Near-ridge 'hot-spots', therefore, may not require the elevated temperatures commonly invoked to account for excess melting. The proposed mechanism also satisfies counterintuitive observations of ridge-bound 'hot-spots' at slow- to intermediate-spreading centres, yet not fast-spreading centres, where large dynamic ridge suction forces likely overwhelm density driven downwellings.

The lack of observations of such downwellings in numerical modelling studies to date, reflects the generally high chemical depletion buoyancy and/or low thermal expansivity parameter values employed in simulations, which we find to be unrepresentative for melting at < 2.3 GPa. We therefore invite future studies to review the values used for parameters affecting density changes during melting (i.e. depletion buoyancy; latent heat of melting; specific heat capacity; thermal expansivity), which quite literally have the potential to turn our understanding of mantle dynamics upside down.

INTRODUCTION

With the development of plate tectonic theory in the 1960's, volcanism occurring away from plate boundaries became recognised as anomalous. Spatially fixed regions of melt generation in the mantle, over which the tectonic plates moved, were thus suggested to account for age progressive intraplate ocean island chains, such as Hawaii (Wilson, 1963). One concept to account for such fixed regions of melt generation below the lithosphere is the mantle plume, i.e. an upwelling of anomalously hot material from the core-mantle boundary (Morgan, 1971). The mantle plume theory has been adopted at many melting anomalies, spanning a wide variety of geologic settings, often negating the direct need for alternative hypotheses to be developed. Consequently, intraplate (and plate boundary) melting anomalies have themselves become known as 'hot-spots'.

'Hot-spots', however, do not consistently demonstrate elevated temperatures and, between studies, source temperature estimates can vary widely for individual 'hot-spots' (e.g. Foulger, 2012). For example, some studies conclude very little difference in source temperature between MORB and Hawaii's 'hot-spot' lavas (e.g. Green and Falloon, 2005), whilst others infer a 235˚C hotter source at Hawaii (Putirka, 2005). If melting anomalies do not demonstrate elevated source temperatures, they cannot be the result of a thermal mantle plume. Furthermore, 'hot-spots' are not fixed. Recently, Hawaii has been found to rapidly drift southwards relative to other Pacific 'hot spots' (Konrad et al., 2018), whilst the Mid Atlantic Ridge-bound Azores 'hot-spot' may be drifting northward (Arnould et al., 2019). At the same time, the Pacific and Atlantic plume groups are well known to move relative to one another (Norton, 2000). Other 'hot-spots' demonstrate complex spatio-temporal evolutions, unexplainable by the classic mantle plume hypothesis, and such examples are prevalent within the West Pacific Seamount Province (e.g. Koppers et al., 2003; Ballmer et al., 2007). In general, 'hot-spots' are observed to be drifting towards spreading centres (Wang et al., 2018) and may demonstrate long-term interactions with spreading centres (Whittaker et al., 2015). If 'hot-spots' drift, feasibly due to mantle plumes interacting with lateral convection currents (e.g. Nolet et al., 2007), this changes the initial assumption that 'hot-spots' are fixed relative to the deep mantle. In addition, uplifted volcanic

regions such as the Southern Sierra Nevada are now generally attributed to delamination of dense magmatic cumulates (e.g. Zandt, 2003), not to mantle plumes. One can, therefore, speculate whether the mantle plume hypothesis would initially have been developed had these realisations been gained earlier.

As such, we take a fresh look at 'hot-spots' and explore a new potential mechanism of generating related melting anomalies. Mechanisms compatible with a potential lack of elevated source temperature at 'hot-spots', a long-term affinity of 'hot-spots' with ocean spreading centres, and 'hot-spot' drift (particularly towards spreading centres), are favourable. Here, we provide an overview of 'hot-spot' locations within the Pacific and Atlantic oceans and demonstrate a preferential association of ridge-bound 'hot-spots' with slow- (10 – 40 mm y^{-1} full spreading rate) to intermediate- (40 – 90 mm y^{-1} full spreading rate) spreading centres, but not fast- (> 90 mm y^{-1} full spreading rate), nor ultra-slow (< 10 mm y^{-1} full spreading rate), spreading centres. To better understand the dynamics behind this association, we review and model the expected changes in density during melting beneath spreading centres. Controversially, when using realistic values for both chemical and thermal parameters controlling density changes during melting, we find that mantle residues increase in density at pressures < 2.3 GPa. The implication that melt residues beneath mid-ocean ridge (MOR) settings may become gravitationally unstable and sink is significant for our understanding of mantle dynamics and may explain anomalous 'hot-spot' magmatism at spreading centres.

'HOT-SPOT' LOCATIONS AND INTERACTIONS WITH OCEAN SPREADING CENTRES

Mantle plumes are commonly assumed to play a central role in continental breakup (i.e. 'Active Rifting' (Sengör and Burke, 1978)), but a minor role in subsequent plate tectonic motions. For example, many 'hot-spots' most arguably linked to mantle plumes are found in intraplate settings (e.g. Hawaii)

and demonstrate little influence on plate boundary locations or plate motions. Instead, slab-pull has been established as the major driving force of plate tectonics for over 40 years (Forsyth and Uyeda, 1975).

Despite mantle plumes playing a minor role in driving plate tectonic motions, many 'hot-spots' (both related and unrelated to past episodes of continental breakup) are located along MORs. This relationship remains the case despite the absolute motion of MORs relative to mantle plume locations, which are generally assumed to be fixed. The association of 'hot-spots' and MORs is most apparent within the slow-spreading Atlantic Ocean (e.g. Whittaker et al., 2015), where proposed distinct near-ridge volcanic anomalies include the Bouvet, Shona, Meteor, Gough, Tristan, St Helena, Ascension, Sierra Leone, 14˚N Anomalies, Atlantic Ridge, Great Meteor, Azores, Iceland, and Jan Mayan 'hot-spots' (Figure 1) (Courtillot et al., 2003; Douglass et al., 1995; Jackson et al., 2017; Long et al., 2019; Montelli et al., 2004; Montelli et al., 2006; Schilling et al., 1994; Steinberger, 2000; Whittaker et al., 2013).

The correlation of 'hot-spots' and ridge axes can be attributed to 'ridge suction' forces, where the replacement of material lost at spreading centres due to lithospheric growth and plate spreading governs the local mantle flow. Ridge suction, therefore, has been postulated to pull mantle plumes towards spreading centres (e.g. Niu and Hékinian, 2004), a process often termed plume 'capture'. Several on-axis 'hot-spots' are speculated to be ridge-captured mantle plumes, including the 14˚N Anomaly (Long et al., 2019) and Galápagos 'hot-spots' (Gibson et al., 2015).

The strength of ridge suction forces are related to ocean spreading rate, where faster plate separation requires a larger replacement of material at the spreading axis, resulting in stronger ridge suction. Therefore, this phenomenon suggests a positive correlation should exist between the number of ridge-captured plumes and the spreading rate of a MOR. Along ultra-slow segments of the SW Indian

ridge and the ultra-slow Arctic spreading centres, a lack of captured 'hot-spots' is consistent with this model (Figure 1). However, when observing the fast-spreading EPR (East Pacific Rise) and the slow-spreading MAR (Mid-Atlantic Ridge), the opposite relationship is apparent. Whilst a predominance of distinct 'hot-spots' can be seen along MAR, a scarcity exists along the EPR (Niu and Hékinian, 2004). 'Hot-spots' that are located near to spreading ridges in the Pacific are found either on slow-intermediate spreading segments of the EPR (e.g. Cobb 'hot-spot', located on the ~25 mm y^{-1} (half spreading rate) segment off the coast of Vancouver, Canada), or on slow-intermediate off-branches of the EPR (e.g. Galápagos 'hot-spot', located along the ~20 mm y^{-1} (half spreading rate) Cocos-Nazca spreading centre) (Figure 1). An apparent exception to this is the Easter Island 'hot-spot', whose associated volcanic ridge is closely affiliated to the Sala y Gómez fracture zone and so the origin of 'hot-spot' magmatism here is disputed (e.g. Morgan, 1971; Clark and Dymond, 1977).

'Hot-spots', therefore, appear to be preferentially located along slow-intermediate spreading centres, and are generally absent from fast-spreading centres, in opposition to the expected effect of ridge suction on buoyant upwelling mantle plumes. Therefore, alternative models for 'hot-spot' generation, that are compatible with the inverse correlation between ridge-bound 'hot-spots' and spreading rate, are required.

DENSITY CHANGES DURING MANTLE MELTING

To understand the relative importance of ridge suction forces in controlling sub-spreading centre mantle flow, it is necessary to quantify other forces of upwelling and downwelling beneath spreading centres. Primarily, these additional forces result from decompression melting, where the mantle residue may become more buoyant due to chemical depletion or increase in density due to cooling.

Negative Density Changes During Melting - Chemical Depletion Buoyancy and Melt Retention

During melting of a fertile mantle source, preferential melting of certain mineral phases (e.g. spinel) drives a systematic shift in the mineralogy of the source rock (Schutt and Lesher, 2006). Overall, a preferential loss of dense phases during melting results in a density decrease of the mantle residue. In addition, compositional changes within the residue further drive a shift to lower densities, due to the preferential loss of dense incompatible elements (e.g. Fe) to the melt fraction. This phenomenon results in chemical depletion buoyancy and, in general, greater degrees of partial melting result in increasingly chemically buoyant mantle residues.

Due to changes in the bulk mineralogy with depth, the magnitude of chemical depletion buoyancy is highly dependent on the ambient pressure during melting, e.g. passing between the spinel and garnet stability fields greatly affects density changes during melting. Attempts to quantify the magnitude of depletion buoyancy vary significantly and earlier studies tended to significantly over or underestimate these. For example, Oxburgh and Parmentier (1977) predicted a density change of ~-0.076 % for each 1 % of melting, whilst Shaw and Jackson (1973) predicted residue densities increase during melting (i.e. the opposite of depletion buoyancy). Recently, work using extensive compilations of mantle mineral physics results has shown modest depletion buoyancies on the order of ~-0.021 % to be representative for melting beneath a MOR (i.e. at ~1 GPa; Schutt and Lesher, 2006).

In addition to depletion buoyancy, the retention of a small volume of low-density melt in the mantle may also contribute to the "overall" residue buoyancy (i.e. combined buoyancy of the residue rock and trapped melt) (e.g. Jha et al., 1994). Pore geometry can influence the ability of melt to migrate to the surface (e.g. Faul, 2001) and melt is retained in the mantle if the porosity remains unconnected i.e. if the dihedral angle (θ) is < 60˚, the permeability is forced to zero (Corderey and Morgan, 1992). Evidence of interconnected melt networks at low partial melt fractions (i.e. < 1 %) is well established from hot pressing experiments, in particular from those using radioactive tracers (e.g. Daines and

Richter, 1988). However, melt viscosity can vary significantly during the melting process and can also affect melt migration. If the viscosity is too high for melt to flow to the surface under its own buoyancy, it may be retained in the mantle. Early melts tend to be rich in volatiles and highly mobile at extremely low melt fractions (~ 0.1 % or less), whilst later basaltic melts of higher viscosity may only become mobile at ~ 1 % melt fraction (Faul, 2001). Whilst estimations of melt fractions retained in the mantle vary widely, between < 0.1 and ~ 3 % (e.g. Schmeling, 1985; Cordery and Morgan, 1992; Faul, 2001; Goes et al., 2012), most estimates suggest mobility at low melt fractions (~0.1 %) is likely (e.g. Lundstrom et al., 1999; Faul, 2001). Furthermore, Goes et al. (2012) demonstrated that the higher volumes (1-3 %) of melt retention often inferred from low seismic velocity observations beneath spreading centres, are likely the result of solid-state seismic attenuation. Therefore, the effect of melt retention on the density of mantle residues can be considered to be small.

Positive Density Changes During Mantle Melting – Thermal Contraction

During decompression melting, mantle residues lose latent heat energy to the melt fraction as phases change state from solid to liquid. As melting progresses, therefore, the latent heat of melting results in cooling and thermal contraction of mantle residue, increasing its density. Previous studies have employed values for the latent heat of melting between 0.73 MJ kg^{-1} (Cordery and Morgan, 1992) and 0.32 MJ kg^{-1} (Schmeling, 2010), where lower values result in less cooling of mantle residue during melting. Realistic values for the latent heat of melting beneath a MOR, however, have been found to lie around the higher end of these values around 0.6 MJ kg^{-1} (Cannat et al., 2004).

For a given heat loss due to the latent heat of melting, the specific heat capacity of mantle material determines the changes in temperature and, therefore, volume and density. Higher heat capacities result in smaller temperature reductions during melting. Common values used in numerical modelling studies range between 1000 and 1300 J kg^{-1} K^{-1} (e.g. Bianco et al., 2013; Brune et al., 2013; Schmeling,

202 2010), where Cannat et al. (2004) found a value of 1200 J kg^{-1} K^{-1} to be appropriate for mantle material
203 beneath a MOR.
204
205 For a given temperature reduction during melting, the thermal expansion coefficient of mantle
206 material controls the change in volume and, therefore, density. A larger thermal expansivity results in
207 greater volume reduction, and therefore density increase, during cooling. The thermal expansivity of
208 mantle material is highly sensitive to pressure, ranging from ~2.4e-5 to 5.2e-5 K^{-1} between the mantle
209 transition zone and the surface, respectively. Values for the thermal expansivity between pressures
210 of 0 and 4.5 GPa are shown in Figure 2d (Katsura, 2010). In low pressure melting environments (such
211 as beneath a MOR), therefore, high thermal expansivities result in relatively large volume reductions
212 and density increases for a given amount of cooling. Previous numerical modelling studies have
213 employed values for thermal expansivity between 3 and 3.7e-5 K^{-1}, which are appropriate for average
214 upper mantle pressures, however, Schutt and Lesher (2006), and Katsura (2010) found a significantly
215 higher value of ~4.9e-5 K^{-1} to be more appropriate beneath a MOR.
216

217 **METHODOLOGY**

218
219 To determine overall density changes during decompression melting of a fertile mantle source, we
220 undertake a literature review to identify the most reasonable values for parameters controlling
221 chemical and thermal density changes of mantle material during melting, as summarised above. The
222 selected values are then used to model density changes during melting using the below equations for
223 chemical and thermal density changes, $\Delta\rho_C$ and $\Delta\rho_T$, respectively:

224 $$\Delta\rho_C = \rho_{ref} \cdot \Delta\rho_{C(\%)}$$

225 (1)

Where ρ_{ref} is the mantle reference density and $\Delta\rho_{C(\%)}$ is the percentage change in chemical density per % of melting.

$$\Delta\rho_T = \rho_{ref} \cdot \Delta T \cdot \alpha \quad (2)$$

Where α is the thermal expansivity and ΔT, the change temperature per % melting, is defined by:

$$\Delta T = \frac{\Delta H_m}{C_p} \cdot 0.01 \quad (3)$$

Where ΔH_m is the latent heat of melting and C_p is the specific heat capacity.

Combing the chemical (1) and thermal density changes (2), gives the total instantaneous change in density during melting:

$$\Delta\rho = \Delta\rho_C + \Delta\rho_T \quad (4)$$

To constrain the chemical density change of mantle against the degree of partial melting, we use the values determined by Schutt and Lesher (2006), which are constrained at pressures of 1, 3, 3.5 and 4 GPa. The best fit curve of Schutt and Lesher (2006) can be reasonably approximated to a linear fit, allowing a simple estimation of density change per % of melting (red lines in Figure 2b).

As large volumes of partial melting are expected at MOR settings (~ 20 %) and residual melt volumes are likely to be extremely low (~ 0.1 %; e.g. Faul, 2001), density changes due to the retained melt fraction are likely to be significantly smaller than those due to chemical density changes. In light of this and the overall poor constraints on retained melt volumes, we do not consider the effects of melt retention any further.

To calculate density changes due to thermal contraction for each % of melting, we use the values for latent heat (0.6 MJ kg^{-1}) and heat capacity (1200 J kg^{-1}) proposed by Cannat et al. (2004) for melting beneath a MOR, which we do not vary with pressure. In addition, we use the pressure dependant thermal expansivity coefficients determined by Katsura et al. (2010), allowing us to model thermal density changes appropriate for the pressures of melting beneath a MOR. We have assumed a reference mantle density of 3300 kg m^{-3} and, for easy comparison with depletion buoyancies predicted by Schutt and Lesher (2006), we show our results at 0, 1, 3, 3.5 and 4 GPa (Figure 2c).

RESULTS

By combining the changes in chemical density predicted by Schutt and Lesher (2006) with our calculated changes in thermal density, we can determine the total instantaneous density changes during melting at different pressures.

Schutt and Lesher (2006) give chemical density changes during melting, which at pressures of 1, 3, 3.5, and 4 GPa (Figure 2a) correspond to density changes of ~-0.021, -0.023, -0.045, and -0.057 % for each 1 % of melting, respectively. At lower pressures (< 3 GPa), therefore, only modest decreases in density result from chemical depletion buoyancy effects during decompression melting.

Our calculations for thermal density changes during melting suggest the largest increases occur at the shallowest depths. At 0 GPa, we predict a 0.026 % change in density for each % of melting. Density changes then decrease with increasing pressure, where at 1, 3, 3.5, and 4 GPa, we predict density changes of 0.0244, 0.0212, 0.0205, and 0.0199 % for each % of melting, respectively (Figure 2c). It is apparent that, assuming realistic values for parameters that determine temperature driven density changes, thermal density changes are on a similar order to depletion buoyancy effects.

Overall Density Changes During Mantle Melting

Using the above determinations of chemical depletion buoyancy and thermal density increases, we calculate the overall density changes of mantle residue resulting from decompression melting. We do this for pressures at which both the chemical depletion buoyancy and thermal expansion effects are constrained, i.e. 1, 3, 3.5, and 4 GPa (Schutt and Lesher, 2006; Katsura et al., 2010) and show these in Figure 2e. In addition, we also calculate a total density change for 0 GPa, where values for the thermal expansivity are constrained by Katsura et al. (2010), by assuming a constant depletion buoyancy effect shallower than 1 GPa, i.e. a -0.021 % density change for each % of melting between 0 and 1 GPa.

We find overall density changes of ~0.005, 0.0034, -0.0019, -0.0245, and -0.0372 % for each % of melting occur at pressures of 0, 1, 3, 3.5, and 4 GPa, respectively (Figure 2e). Therefore, at greater depths our results concur with the general assumption that mantle residues decrease in density upon melting. In contrast to previous studies, however, we predict a switch from decreasing to increasing residue densities where melting occurs at pressures of less than 2.3 GPa.

The predicted overall increase in density of mantle residues during shallow melting contradicts the common assumption that residues ubiquitously decrease in density upon melting. However, this assumption has been based on values for depletion buoyancy and thermal parameters which, in some instances, are outdated or representative of average upper mantle pressures (~3-15 GPa) and not pressures < 3 GPa, where the predominance of melting occurs. Niu and Batiza (1991) also investigated density changes at lower pressures and found a small decrease in residue density upon melting. However, this study neglected the pressure effect on thermal expansivity, which we find here to be a key contributor to increasing residue densities upon melting.

DISCUSSION

Mantle Dynamics During Melting and Near-ridge 'Hot-spots'

As large changes in the physical properties of upper mantle occur during melting, it is important to understand the likely impact of these changes for mantle dynamics when interpreting the cause of excess melting at 'hot-spots'. Above, we determined that increases in the residue density occur during melting at pressures lower than 2.3 GPa (Figure 2e). Such pressures exist within the asthenosphere beneath rifts, spreading centres, and young ocean. Assuming the base of oceanic lithosphere approximately follows the 1200˚C isotherm (e.g. Kawakatsu et al., 2009), this crosses the 2.3 GPa isobar after ~40 Ma (Figure 2f). Both the greatest degrees of partial melting and the largest density increases per % of melting occur at the shallowest depths beneath MORs. Therefore, density increases are most likely to have the greatest effect in the lowest pressure region directly beneath a spreading axis.

Dense mantle residues are gravitationally unstable and Rayleigh-Taylor instabilities are, therefore, likely to develop beneath spreading centres, i.e. mantle downwellings. Such downwellings would be replenished by freshly melted dense mantle residues from above, which in turn would be replaced laterally by fertile asthenosphere undergoing melting (Figure 3b). Marquart (2001) showed that mantle flow beneath even a simple linear MOR does not conform to a simple 2D flow pattern, i.e. equal upwelling rates along the length of the ridge. Instead, upwellings preferentially develop at localised points along the ridge at intervals of ~500 km, not dissimilar to the spacing of some 'hot-spots' along the MAR. We propose a similar, but inverted, flow pattern for sinking dense mantle residues beneath MORs, where point locations of enhanced downwelling generate observed 'hot-spots'. Ridge-perpendicular Richter Rolls have previously been invoked to explain enhanced mantle flow away from a ridge axis (e.g. Ballmer et al., 2007; Marquart, 2001) and similar flow patterns may contribute to the enhancement of off-axis volcanism associated with downwelling residues.

Downward forces due to increases in density are, however, not the only forces influencing sub-spreading centre dynamics and ridge suction forces also need to be considered.

Ridge suction forces pull mantle asthenosphere into the spreading ridge to replace the volume lost due to plate separation. These suction forces act in the generally opposite sense to density driven sinking. The two forces, therefore, are in competition (see black and blue arrows, Figure 2f). Due to large uncertainties in the viscosity of asthenospheric mantle (of over an order of magnitude, e.g. Doglioni et al., 2011; James et al., 2009) it is difficult to quantify the interplay of these forces. However, it is clear that ridge suction forces are stronger at fast-spreading centres and, therefore, fast-spreading rates are more likely to overwhelm density driven downwellings (Figure 3a). Consequently, downwellings are most likely to occur where spreading rates are low to moderate (Figure 3b), consistent with the prolificacy of 'hot-spots' along the slow-spreading Mid-Atlantic Ridge and general lack of 'hot-spots' along fast-spreading segments of the East Pacific Rise.

At ultra-slow spreading ridges, a general paucity of 'hot-spots' is also observed, e.g. along the ultra-slow Arctic Ridge. However, this is consistent with our downwelling driven 'hot-spot' model, as dense residue downwellings are unlikely to develop in these settings for several reasons: 1) the cooler lithosphere extends deeper into the mantle and so partial melting occurs at higher pressures, resulting in lower density increases, 2) ultra-slow spreading ridges undergo very low degrees of partial melting, leading to small total density increases of mantle residue, which may be insufficient to instigate downwelling, and 3) the basal geometry of lithosphere beneath ultra-slow spreading centres is steep sided and, depending on asthenospheric viscosity, downwelling currents may not "fit alongside" necessary ridge suction flows (Figure 3c).

Mantle Downwellings and 'Hot-spots'

The concept of producing excess melt due to mantle downwellings provides an efficient mechanism to explain the origin of 'hot-spots' and has been suggested in many forms since the development of plate tectonic theory. Shaw and Jackson (1973) propose that mantle downwellings (i.e. "gravitational anchors") generated the Hawaiian 'hot-spot' chain. Similar to the mechanism proposed here, Shaw and Jackson proposed gravitational anchors form due to an increase in mantle residue density upon melting. We emphasise, however, that this early study suggested residue density increases resulted directly from chemical depletion, which is in disagreement with more recent literature and our own findings. More recently, Keen and Boutilier (1995) and King and Anderson (1995) have suggested that small-scale convection, driven by cool downwellings of asthenosphere adjacent to continental margin thermal gradients, can produce the excess melting observed during magma-rich continental breakup. King (2007) expanded on this concept to suggest that edge-driven convection may also occur adjacent to cratonic roots, potentially explaining many intraplate melting anomalies. Similarly, the delamination and sinking of dense lithospheric material has been suggested to account for uplift and magmatism at Afar (e.g. Esedo et al., 2012), East Anatolia (Keskin, 2007), and the Colorado Plateau (e.g. Levander et al., 2011). It is clear, therefore, that the concept of downwelling mantle resulting in a 'hot-spot' is not unfamiliar. Here, we propose a fundamental re-envisioning of mantle dynamics during melting at shallow depths (< 2.3 GPa) capable of producing 'hot-spots' i.e. dense residue downwellings, as opposed to buoyant residue upwellings. Such downwellings are likely to be self-sustaining and may produce long-lived melting anomalies. Our model may, therefore, account for ocean island chains characteristic of 'hot-spots' and do not invoke a deep mantle source, compatible with the low He ratios observed at many 'hot-spots' (e.g. Jackson et al., 2017).

Whilst our arguments explicitly account for the general distribution of 'hot-spots' at ultra-slow, slow-intermediate, and fast-spreading centres, we do not attempt to account for the irregular distributions of 'hot-spots' along slow-intermediate spreading centres. Although a full analysis of the factors controlling the local distributions of 'hot-spots' along the MAR is beyond the scope of this study, we

propose that local variations in mantle chemistry, spreading centre geometry/transform offsets, and regional mantle winds, likely play a role. In the spirit of this volume, we leave this question for future workers to investigate further.

Applicability of Mantle Downwellings to Deeper (Non-rift/ridge) Melting Anomalies

The controversial finding that mantle residues become instantaneously denser following melting at shallow depths (< 2.3 GPa) is based on the most realistic values for parameters controlling density changes during melting (i.e. chemical depletion buoyancy, thermal expansivity, latent heat of melting, and specific heat capacities) identified by this study. Where variations in parameter estimates exist within the literature, we have taken the more recent of these to be the most reliable or have selected only modest values within the range suggested by the literature. Nonetheless, as these parameters are difficult to determine for mantle conditions, each parameter comes with a (sometimes large) range of error, of which the depletion buoyancy estimates are the most significant (i.e. grey bands, Figure 2b).

At a pressure of 1 GPa, the predicted range of error in Schutt and Lesher's (2006) chemical buoyancy determinations extends from -0.013 % to -0.029 % for each 1 % of melting. Taking the lower estimate (-0.013 %), the expected chemical buoyancy is reduced, which further increases the total density of mantle residues due to melting (0.0114 % instead of 0.0034 % for each 1 % of melting). Taking the higher estimate (-0.029 %), however, results in a greater chemical buoyancy and mantle residues become buoyant overall (-0.0046 % as opposed to 0.0034 %). Within the error range predicted by Schutt and Lesher (2006), therefore, neither behaviour of mantle residue (buoyancy uplift vs density sinking) can be ruled out at 1 GPa. The best fit case and majority of potential values, however, indicate that residues instantaneously increase in density upon melting.

At pressures of 3 GPa, we have predicted that residues become slightly less dense upon melting. The predicted range of error in Schutt and Lesher's (2006) chemical buoyancy values here are larger than those at 1 GPa, and extend from -0.01 % to -0.036 % for each 1 % of melting. Taking the lower estimate (-0.01 %) the chemical buoyancy is reduced and thermal density effects again dominate. Mantle residues, therefore, may still become significantly denser overall (0.0112 % for each 1 % of melting as opposed to -0.0019 %) at these pressures. Taking the higher estimate (-0.036 %) further increases chemical buoyancy and results in strongly buoyant mantle residues (-0.0149 % as opposed to -0.0019 %). Within the range of error, therefore, both behaviours of mantle residues (buoyancy uplift and density sinking) are also possible at 3 GPa, although the majority of potential values indicate residues become less dense.

Deeper than 3 GPa, the high values of depletion buoyancy and low thermal expansivities result in buoyant melt residue predictions across the full error range predicted by Schutt and Lesher (2006) for depletion buoyancies. Therefore, under certain conditions dense residues may be produced by melting around or shallower than 3 GPa, but not significantly below. As oceanic lithosphere does not exceed pressures of 3 GPa (e.g. Niu and Green, 2018), it is within the error of our modelling for melting below any oceanic region to result in dense residue production. It is possible, therefore, that all melting anomalies found within the oceanic domain may be the result of dense mantle residue downwellings. This could explain the presence of non-age progressive volcanic chains in the old oceanic lithosphere of the West Pacific (e.g. Koppers et al., 2003), which are difficult to reconcile with the traditional mantle plume model.

Implications for Numerical Modelling Studies

Significant advances in numerical codes for geodynamic modelling over the past few decades have led to the integration of many new features to better account for the full behaviour of geodynamic

429 processes, for instance: non-linear and visco-elasto-plastic rheologies (e.g. Gerya and Yuen, 2007;
430 Glerum et al., 2018). Such features allow a better approximation of the Earth's behaviour and as a
431 community it is important to continue improving these. To the same end, however, it is important to
432 continuously review our understanding of parameters for well-established features of numerical
433 models, such as buoyancy factors during melting. Considering this, we have reviewed the parameters
434 controlling density changes during mantle melting for a selection of numerical modelling studies and,
435 where these values have been provided, we report them in Table 1. Whilst the parameter values used
436 can vary significantly between studies, possibly to reflect specific study settings, we find that many
437 align with our own findings. In no case, however, does a single study use all parameter values in
438 general alignment with the most reasonable values determined here. As a result, we find that all
439 numerical studies reviewed here produce instantaneously buoyant melt residues upon melting, in line
440 with the existing paradigm. It is not surprising, therefore, that no numerical modelling study (to our
441 knowledge) has yet predicted melting anomalies related to our proposed dense residue downwellings.
442
443 Across the reviewed studies, varying combinations of values for thermal expansivity, chemical
444 depletion buoyancy, latent heat of melting, and specific heat capacities result in the production of
445 buoyant mantle residues. However, of greatest significance are the values use for thermal expansivity.
446 Across all studies, these range between 3×10^{-5} K^{-1} (e.g. Brune et al., 2013) and 3.7×10^{-5} K^{-1} (e.g.
447 Schmeling, 2010). Significantly lower than the $4.2 - 5.2 \times 10^{-5}$ K^{-1} representative for depths < 3 GPa (e.g.
448 Katsura et al., 2010), where the majority of melting occurs. To emphasise the effect of this, changing
449 the thermal expansivity within a numerical model from 3×10^{-5} K^{-1} to 4.9×10^{-5} K^{-1} results in a 63 %
450 increase in thermal density effects during melting. Revising this factor alone may, therefore, result in
451 many numerical modelling studies predicting inverted convection beneath ridges during melting
452 (perhaps observations of this 'absurd' geodynamic behaviour has itself inhibited the revision of this
453 parameter in some studies?).
454

Similarly, the coefficients for depletion buoyancy used across numerical studies also vary considerably. These range from -0.022 % (e.g. Ballmer et al., 2007) to -0.085 % density change for each 1 % of melting (Schmeling, 2010), with the majority of studies using values between -0.04 % and -0.06 %. Therefore, whilst some studies use values consistent with Schutt and Lesher's (2006) suggestion of between -0.021 and -0.023 % density change for each 1 % of melting (at pressures < 3 GPa), most invoke significantly larger depletion buoyancy factors. The significance of depletion buoyancy in controlling total density changes during melting are self-evident, where changing this parameter from a value of -0.085 to -0.021 reduces the buoyancy of residues by over a factor of 4.

Values used for the latent heat of melting (or entropy of melting) range from 0.32 MJ kg^{-1} (Schmeling, 2010) to 0.73 MJ kg^{-1} (Bianco et al., 2013; Cordery and Morgan, 1992), either side of the 0.6 MJ kg^{-1}, suggested by Cannat et al. (2004). The latent heat of melting is a critical parameter in determining density changes upon melting and, whilst many studies do not quote the values used, we find that most values lie in the vicinity of the 0.6 MJ kg^{-1} proposed here. Similarly, the specific heat capacity shows the lowest variability across studies, ranging between 1000 J kg^{-1} K^{-1} (e.g. Cordery and Morgan, 1992) and 1300 J kg^{-1} K^{-1} (e.g. Schmeling, 2010). In agreement with our findings, the majority of studies employ a value of 1200 J kg^{-1} K^{-1}.

The values chosen for the above parameters have the potential to significantly change geodynamic behaviours observed in numerical models. Changing a single parameter to (what we suggest as) a more likely value can alone result in denser, as opposed to more buoyant, mantle residues. Such residues sink into the mantle and do not buoyantly float as widely assumed. In future modelling studies, therefore, we invite reconsideration of the values used for these parameters.

CONCLUSIONS

In reviewing the material properties responsible for density changes during decompression melting of a fertile mantle source (i.e. thermal expansivity, chemical depletion buoyancy, latent heat of melting, and specific heat capacity), we find overall density changes of 0.005, 0.0034, -0.0019, -0.0245, and -0.0372 % for each % of melting at pressures of 0, 1, 3, 3.5, and 4 GPa, respectively. At shallow depths (< 2.3 GPa), therefore, we predict that melt residues instantaneously increase in density during melting. This controversial finding is due to thermal contraction of material during melting, which at shallow pressures (where thermal expansivities are highest), outweighs the chemical buoyancy due to melting. The generation of self-sustaining mantle downwellings beneath shallow melting regions is, therefore, predicted and such downwellings may locally enhance melt production by increasing the flow of fertile asthenospheric mantle through the melting window. These dense residue downwellings may explain the presence of long-lived melting anomalies along the Mid-Atlantic Ridge, where shallow melting anomalies are abundant and only modest ridge suction forces exist to counteract dense residue downwellings. By reviewing the distribution of 'hot-spots' along the global ocean spreading centre network, we furthermore observe a general lack of 'hot-spots' at both fast- and ultra-slow spreading centres. We attribute this to strong ridge suction forces (overwhelming density driven sinking) and low volumes of deep melting (producing only small fractions of modestly dense residue), respectively. Within error, dense melt residues may be predicted down to depths of 3 GPa, potentially accounting for all observed 'hot-spot' melting anomalies within ocean basins, although probably not for cratonic continental settings. Our findings suggest that 'hot-spots', particularly in regions of thin lithosphere, are not necessarily the result of hot mantle plumes, but instead might originate from cool residue downwellings. Our review of a selection of numerical modelling studies highlights the general use of values for key mantle properties that result in buoyant mantle residues during melting,

503 explaining the lack of observed dense downwellings in numerical studies to date. We, therefore, invite
504 future studies to reconsider the values used for these parameters as they, quite literally, have the
505 potential to turn our understanding of mantle dynamics upside down.
506

507 **ACKNOWLEDGEMENTS**

508

509 We would like to thank Sorin Barzoi and James Natland for their constructive comments which
510 significantly improved this manuscript. The ocean spreading rate data and hotspot compilations used
511 in this study were obtained freely from EarthBYTE (https://www.earthbyte.org/gplates-2-2-software-
512 and-data-sets/).
513

514 **REFERENCES**

515

516 Armitage, J.J., Henstock, T.J., Minshull, T.A. and Hopper, J.R., 2008. Modelling the composition of melts
517 formed during continental breakup of the Southeast Greenland margin. *Earth and Planetary*
518 *Science Letters*, *269*(1-2), pp.248-258.
519

520 Arnould, M., Ganne, J., Coltice, N. and Feng, X., 2019. Northward drift of the Azores plume in the
521 Earth's mantle. *Nature communications*, *10*(1), pp.1-8.
522

523 Ballmer, M.D., van Hunen, J., Ito, G., Tackley, P.J. and Bianco, T.A., 2007. Non-hotspot volcano chains
524 originating from small-scale sublithospheric convection. *Geophysical Research Letters*, *34*(23).
525

526 Bianco, T.A., Ito, G., van Hunen, J., Mahoney, J.J. and Ballmer, M.D., 2013. Geochemical variations at
527 ridge-centered hotspots caused by variable melting of a veined mantle plume. Earth and
528 Planetary Science Letters, 371, pp.191-202.
529
530 Brune, S., Popov, A.A. and Sobolev, S.V., 2013. Quantifying the thermo-mechanical impact of plume
531 arrival on continental break-up. *Tectonophysics*, *604*, pp.51-59.
532
533 Burg, J.P. and Gerya, T.V., 2005. The role of viscous heating in Barrovian metamorphism of collisional
534 orogens: thermomechanical models and application to the Lepontine Dome in the Central
535 Alps. Journal of Metamorphic Geology, 23(2), pp.75-95.
536
537 Cannat, M., Cann, J. and Maclennan, J., 2004. Some hard rock constraints on the supply of heat to
538 mid-ocean ridges. *Mid-Ocean Ridges: Hydrothermal Interactions Between the Lithosphere and*
539 *Oceans*, *148*, pp.111-149.
540
541 Clark, J.G. and Dymond, J., 1977. Geochronology and petrochemistry of Easter and Sala y Gomez
542 Islands: Implications for the origin of the Sala y Gomez Ridge. *Journal of Volcanology and*
543 *Geothermal Research*, *2*(1), pp.29-48.
544
545 Cordery, M.J. and Morgan, J.P., 1992. Melting and mantle flow beneath a mid-ocean spreading
546 center. *Earth and planetary science letters*, *111*(2-4), pp.493-516.
547
548 Courtillot, V., Davaille, A., Besse, J. and Stock, J., 2003. Three distinct types of hotspots in the Earth's
549 mantle. *Earth and Planetary Science Letters*, *205*(3-4), pp.295-308.
550

551 Daines, M.J., and Richter, F.M., 1988. An experimental method for directly determining the
552 interconnectivity of melt in a partially molten system. *Geophysical Research Letters,* 15(13),
553 pp.1459-1462.
554
555 Doglioni, C., Ismail-Zadeh, A., Panza, G. and Riguzzi, F., 2011. Lithosphere–asthenosphere viscosity
556 contrast and decoupling. *Physics of the Earth and Planetary Interiors*, *189*(1-2), pp.1-8.
557
558 Douglass, J., Schilling, J.G., Kingsley, R.H. and Small, C., 1995. Influence of the discovery and Shona
559 mantle plumes on the southern Mid-Atlantic Ridge: Rare earth evidence. *Geophysical research*
560 *letters*, *22*(21), pp.2893-2896.
561
562 Esedo, R., van Wijk, J., Coblentz, D. and Meyer, R., 2012. Uplift prior to continental breakup: Indication
563 for removal of mantle lithosphere?. *Geosphere*, *8*(5), pp.1078-1085.
564
565 Faul, U. H., 2001. Melt retention and segregation beneath mid-ocean ridges. *Nature, 410,* pp.920-923.
566
567 Foulger, G.R., 2012. Are 'hot spots' hot spots?. *Journal of Geodynamics*, *58*, pp.1-28.
568
569 Forsyth, D. and Uyeda, S., 1975. On the relative importance of the driving forces of plate
570 motion. *Geophysical Journal International*, *43*(1), pp.163-200.
571
572 Fowler, C.M.R., 2005. The solid Earth – an introduction to global geophysics, 2nd Edition. Cambridge
573 University Press, New York (685 pp)
574

575 Gerya, T. V. and Yuen, D. A.: Robust characteristics method for modelling multiphase visco-elasto-
576 plastic thermo-mechanical problems, Physics of the Earth and Planetary Interiors, 163, 83–
577 105, 2007.
578
579 Gibson, S.A., Geist, D.J. and Richards, M.A., 2015. Mantle plume capture, anchoring, and outflow
580 during Galápagos plume-ridge interaction. *Geochemistry, Geophysics, Geosystems*, *16*(5),
581 pp.1634-1655.
582
583 Glerum, A., Thieulot, C., Fraters, M., Blom, C. and Spakman, W., 2018. Nonlinear viscoplasticity in
584 ASPECT: benchmarking and applications to subduction. *Solid Earth*, *9*, pp.267-294.
585
586 Goes, S., Armitage, J., Harmon, N., Smith, H., Huismans, R., 2012. Low seismic velocities below mid-
587 ocean ridges: Attenuation versus melt retention. *Journal of Geophysical Research: Solid Earth,*
588 *117(B12)*.
589
590 Green, D.H. and Falloon, T.J., 2005. Primary magmas at mid-ocean ridges," hotspots," and other
591 intraplate settings: Constraints on mantle potential temperature. *Special Papers-Geological*
592 *Society of America*, *388*, p.217.
593
594 Jackson, M.G., Konter, J.G. and Becker, T.W., 2017. Primordial helium entrained by the hottest mantle
595 plumes. *Nature*, *542*(7641), pp.340-343.
596
597 James, T.S., Gowan, E.J., Wada, I. and Wang, K., 2009. Viscosity of the asthenosphere from glacial
598 isostatic adjustment and subduction dynamics at the northern Cascadia subduction zone,
599 British Columbia, Canada. *Journal of Geophysical Research: Solid Earth*, *114*(B4).
600

601 Jha, K., Parmentier, E. M., Morgan, J. P., 1994. The role of mantle-depletion and melt-retention
602 buoyancy in spreading-center segmentation. *Earth and Planetary Science Letters, 125,* pp.221-
603 234.
604
605 Katsura, T., Yoneda, A., Yamazaki, D., Yoshino, T. and Ito, E., 2010. Adiabatic temperature profile in
606 the mantle. *Physics of the Earth and Planetary Interiors*, *183*(1-2), pp.212-218.
607
608 Kawakatsu, H., Kumar, P., Takei, Y., Shinohara, M., Kanazawa, T., Araki, E. and Suyehiro, K., 2009.
609 Seismic evidence for sharp lithosphere-asthenosphere boundaries of oceanic
610 plates. *Science*, *324*(5926), pp.499-502.
611
612 Keen, C.E. and Boutilier, R.R., 1995. Lithosphere-asthenosphere interactions below rifts. In *Rifted*
613 *Ocean-continent boundaries* (pp. 17-30). Springer, Dordrecht.
614
615 Keskin, M., 2007. Eastern Anatolia: a hotspot in a collision zone without a mantle plume. *Special*
616 *Papers-Geological Society of America*, *430*, p.693.
617
618 King, S.D., 2007. Hotspots and edge-driven convection. *Geology*, *35*(3), pp.223-226.
619
620 Konrad, K., Koppers, A.A., Steinberger, B., Finlayson, V.A., Konter, J.G. and Jackson, M.G., 2018. On the
621 relative motions of long-lived Pacific mantle plumes. *Nature communications*, *9*(1), pp.1-8.
622
623 Koppers, A.A., Staudigel, H., Pringle, M.S. and Wijbrans, J.R., 2003. Short-lived and discontinuous
624 intraplate volcanism in the South Pacific: Hot spots or extensional volcanism?. *Geochemistry,*
625 *Geophysics, Geosystems*, *4*(10).
626

627 Levander, A., Schmandt, B., Miller, M.S., Liu, K., Karlstrom, K.E., Crow, R.S., Lee, C.T. and Humphreys,
628 E.D., 2011. Continuing Colorado plateau uplift by delamination-style convective lithospheric
629 downwelling. *Nature*, *472*(7344), pp.461-465.
630
631 Long, X., Geldmacher, J., Hoernle, K., Hauff, F., Wartho, J.A., Garbe-Schönberg, D. and Grevemeyer, I.,
632 2019. Age and origin of Researcher Ridge and an explanation for the 14° N anomaly on the
633 Mid-Atlantic Ridge by plume-ridge interaction. *Lithos*, *326*, pp.540-555.
634
635 Lundstrom, C.C., Gill, J. and Williams, Q., 2000. A geochemically consistent hypothesis for MORB
636 generation. *Chemical Geology*, *162*(2), pp.105-126.
637
638 Marquart, G., 2001. On the geometry of mantle flow beneath drifting lithospheric plates. Geophysical
639 Journal International, 144(2), pp.356-372.
640
641 Montelli, R., Nolet, G., Dahlen, F.A. and Masters, G., 2006. A catalogue of deep mantle plumes: New
642 results from finite-frequency tomography. *Geochemistry, Geophysics, Geosystems*, *7*(11).
643
644 Montelli, R., Nolet, G., Dahlen, F.A., Masters, G., Engdahl, E.R. and Hung, S.H., 2004. Finite-frequency
645 tomography reveals a variety of plumes in the mantle. *Science*, *303*(5656), pp.338-343.
646
647 Morgan, J.P., 2001. Thermodynamics of pressure release melting of a veined plum pudding
648 mantle. *Geochemistry, Geophysics, Geosystems*, *2*(4).
649
650 Morgan, W.J., 1971. Convection plumes in the lower mantle. Nature 230, 42–43.
651

652 Niu, Y. and Batiza, R., 1991. In situ densities of MORB melts and residual mantle: Implications for
653 buoyancy forces beneath mid-ocean ridges. *The Journal of Geology*, *99*(5), pp.767-775.
654
655 Niu, Y. and Green, D.H., 2018. The petrological control on the lithosphere-asthenosphere boundary
656 (LAB) beneath ocean basins. *Earth-Science Reviews*, *185*, pp.301-307.
657
658 Niu, Y., Hékinian, R., 2004. Ridge suction drives plume-ridge interactions. In Oceanic hotspots (285-
659 307). Springer, Berlin, Heidelberg.
660
661 Nolet, G., Allen, R. and Zhao, D., 2007. Mantle plume tomography. *Chemical Geology*, *241*(3-4),
662 pp.248-263.
663
664 Norton, I.O., 2000. Global hotspot reference frames and plate motion. *The history and dynamics of*
665 *global plate motions*, *121*, pp.339-357.
666
667 Oxburgh, E.R. and Parmentier, E.M., 1977. Compositional and density stratification in oceanic
668 lithosphere-causes and consequences. *Journal of the Geological Society*, *133*(4), pp.343-355.
669
670 Putirka, K.D., 2005. Mantle potential temperatures at Hawaii, Iceland, and the mid-ocean ridge
671 system, as inferred from olivine phenocrysts: Evidence for thermally driven mantle
672 plumes. *Geochemistry, Geophysics, Geosystems*, *6*(5).
673
674 Schilling, J.G., Hanan, B.B., McCully, B., Kingsley, R.H. and Fontignie, D., 1994. Influence of the Sierra
675 Leone mantle plume on the equatorial Mid-Atlantic Ridge: A Nd-Sr-Pb isotopic study. *Journal*
676 *of Geophysical Research: Solid Earth*, *99*(B6), pp.12005-12028.
677

678 Schmeling, H., 2010. Dynamic models of continental rifting with melt
679 generation. *Tectonophysics*, *480*(1-4), pp.33-47.
680
681 Schmeling, H., 1985. Partial melt below Iceland: A combined interpretation of seismic and conductivity
682 data. *Journal of Geophysical Research: Solid Earth, 90(B12),* pp.10105-10116.
683
684 Schutt, D.L. and Lesher, C.E., 2006. Effects of melt depletion on the density and seismic velocity of
685 garnet and spinel lherzolite. *Journal of Geophysical Research: Solid Earth*, *111*(B5).
686
687 Sengör, A.M.C., Burke, K., 1978. Relative timing of rifting and volcanism on Earth and its tectonic
688 applications. Geophys. Res. Lett., 5, 419-421.
689
690 Shaw, H.R. and Jackson, E.D., 1973. Linear island chains in the Pacific: result of thermal plumes or
691 gravitational anchors?. *Journal of Geophysical Research*, *78*(35), pp.8634-8652.
692
693 Steinberger, B., 2000. Plumes in a convecting mantle: Models and observations for individual
694 hotspots. *Journal of Geophysical Research: Solid Earth*, *105*(B5), pp.11127-11152.
695
696 Wang, S., Yu, H., Zhang, Q. and Zhao, Y., 2018. Absolute plate motions relative to deep mantle
697 plumes. *Earth and Planetary Science Letters*, *490*, pp.88-99.
698
699 Whittaker, J.M., Afonso, J.C., Masterton, S., Müller, R.D., Wessel, P., Williams, S.E. and Seton, M., 2015.
700 Long-term interaction between mid-ocean ridges and mantle plumes. *Nature*
701 *Geoscience*, *8*(6), pp.479-483.
702

Whittaker, J. M., Williams, S. E., Masterton, S. M., Afonso, J. C., Seton, M., Landgrebe, T.C., Coffin, M.F., Müller, R.D. 2013. Interactions among plumes, mantle circulation and mid-ocean ridges, AGU Fall Meeting Abstracts.

Wilson, J.T., 1963. A possible origin of the Hawaiian Islands. Can. J. Phys. 41, 863–870.

Zandt, G., 2003. The southern Sierra Nevada drip and the mantle wind direction beneath the southwestern United States. International Geology Review, 45(3), pp.213-224.

729 **TABLE 1. KEY PARAMETER VALUES USED IN NUMERICAL MODELLING STUDIES**

Chemical depletion buoyancy (% change in ρ for each 1% of melting)	Latent heat of melting (MJ kg^{-1})	Specific heat capacity (J kg^{-1} K^{-1})	Thermal expansivity (10^{-5} K^{-1})	Total Density Change (% for each 1% of melting)	Author, year
-0.021			**4.91 (1GPa)**		**Schutt & Lescher, 2006**
	0.6	**1200**		**+0.0036**	**Cannat et al., 2004**
			5.2 – 4.2 (0 - 3 GPa)		**Katsura et al., 2010**
-0.04	0.4 (250 J / kg °C | 1598 K)	1200	3.3	-0.029	Armitage, 2008
-0.022	–	–	3.1	–	Ballmer et al., 2007
–	–	1000	–	–	Bianco et al., 2013
–	–	1200	3.0	–	Brune et al., 2013
–	–	1000	3.0	–	Burg and Gerya, 2005
–	0.73 (450 J / kg °C | 1613 K)	1000	–	–	Cordery and Morgan, 1992
–	–	1250	3.5	–	Mittelstaedt et al., 2011
–	0.66	1200	3.0	–	Morgan, 2001
-0.04	0.64 (400 J / kg °C | 1598 K)	1200	3.3	-0.022	Nielsen and Hopper 2004
–	0.42	1050	3.25	–	Reid and Jackson, 1981
-0.07	–	–	3.5	–	Ribe & Christensen, 1999
-0.085	0.32	1300	3.7	-0.076	Schmeling, 2010
–	–	1200	3.1	–	Simon et al., 2009

730

731 **Table 1.** Values for parameters affecting melt residue density determined and/or used by previous
732 studies. The values determined in studies 1-3 (first three rows, in bold) are considered by this study
733 as the most reliable values for parameters available at this time. Values used by a selection of
734 numerical modelling studies are presented below the solid black line. In general, numerical modelling

735 studies use values more likely to result in buoyant melt residues than those determined herein. In
736 particular, more negative values for chemical depletion buoyancy and lower values for thermal
737 expansivity play a key role. No numerical modelling study, as far as we can determine, uses parameter
738 values that would result in dense melt residues (column 5).
739
740 Latent heat of melting values are presented in black in units of MJ kg^{-1}. Where these have been
741 converted from entropies of melting (in J / kg °C), the original entropy value and the temperature at
742 which the conversion was undertaken (relating to the model domain potential T_{max}) follow in grey.
743 Due to the conversion using the potential T_{max}, latent heat estimates derived in this way likely
744 represent slight over-estimations.
745
746
747

Figure 1

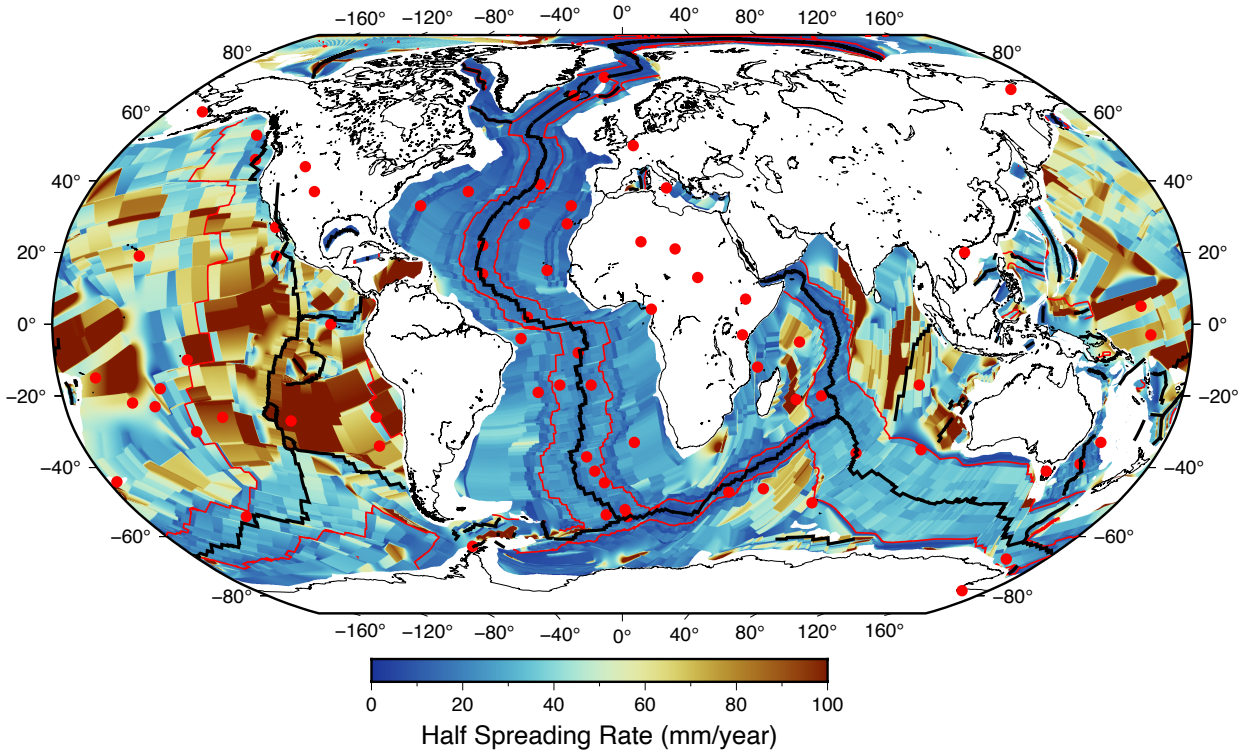

Figure 1: Global half spreading rate of the oceans overlain with 'hot-spot' locations (red circles). Red line delineates 40 Ma old oceanic lithosphere. Near-ridge 'hot-spots' are common in slow-intermediate spreading regions (e.g. Atlantic Ocean) but missing from fast-spreading centres (e.g. Central Pacific), opposite to expectations due to 'ridge suction' effects. A possible exception to this, the Easter 'hot-spot', is related to the Sala y Gómez fracture zone and its origin is disputed. Oceanic crust age and spreading rate data is from Müller et al. (2008). 'Hot-spot' catalogue modified from Whittaker et al. (2013) to include those of Courtillot et al. (2003); Douglass et al. (1995); Jackson et al. (2017); Long et al. (2019); Montelli et al. (2004); Montelli et al. (2006); Schilling et al. (1994); Steinberger (2000).

763 **Figure 2**

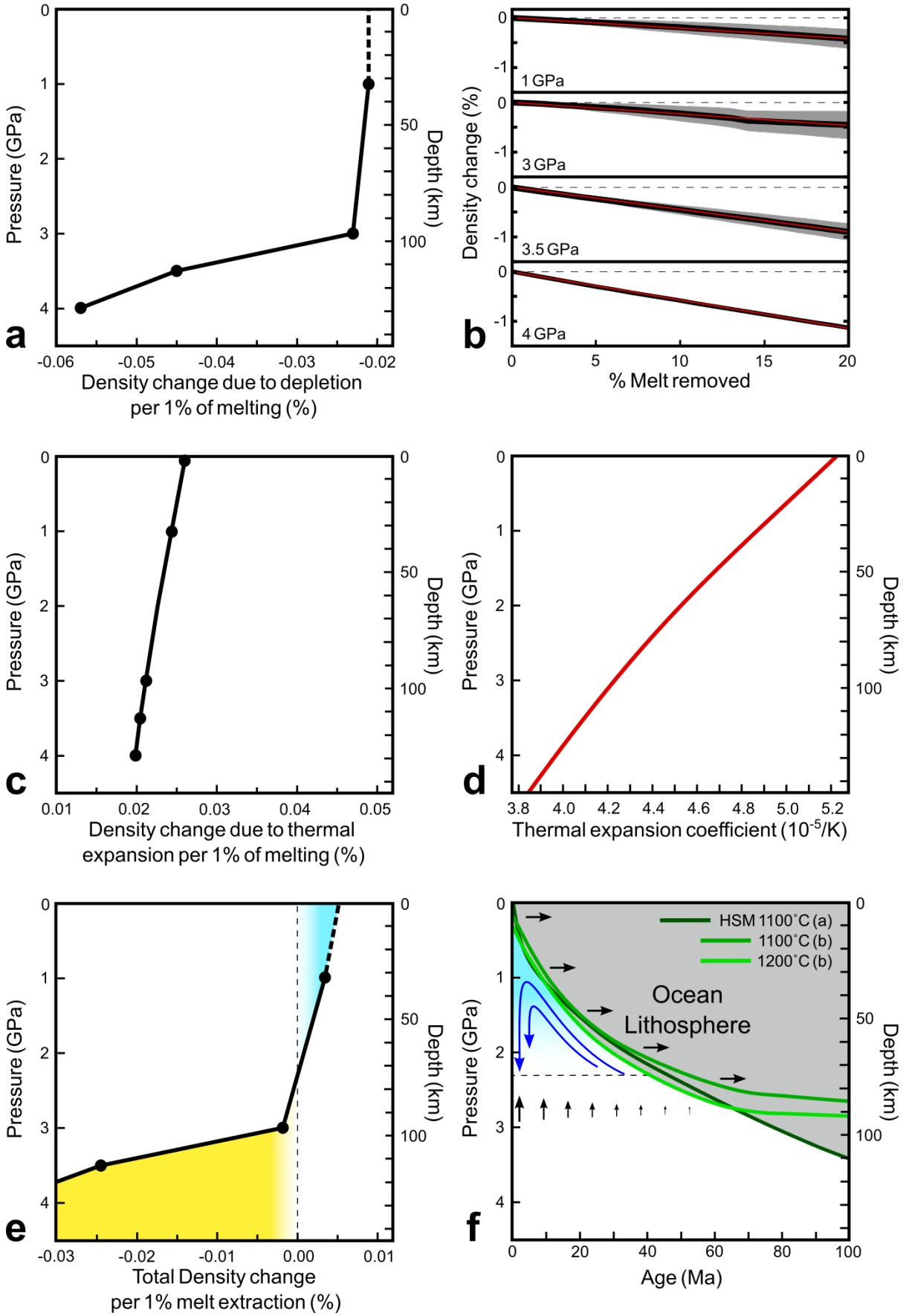

764

765

766 **Figure 2.** Factors influencing mantle residue density changes during decompression melting and
767 spatial extents of dense melt residues. **a)** Variation in density change with depth due to chemical
768 depletion (per % melting) assuming linear approximations shown in **b)** Density change due to chemical
769 depletion buoyancy during 0-20 % melting of mantle at 1, 3, 3.5 and 4 GPa (modified from Schutt and
770 Lesher, 2006). Solid black line = calculated density change, grey band = error, red lines = linear
771 approximation used in (a). **c)** Variation in density change with depth (per % melting) due to cooling
772 during decompression melting and variable thermal expansivity. Density changes determined using a
773 latent heat of melting of 0.6 MJ kg^{-1} (Cannat et al. 2004), specific heat capacity of 1200 J kg^{-1} K^{-1} (e.g.
774 Cannat et al., 2004; Brune et al., 2013), and thermal expansivities shown in **d)** Change in the thermal
775 expansion coefficient for mantle material with depth (Katsura et al., 2010). **e)** Total change in density
776 during melting due to chemical depletion (a) and thermal contraction (c). At depths < 2.3 GPa, mantle
777 residue becomes denser during melting (light blue areas). At depths > 2.3 GPa, mantle residue
778 becomes buoyant during melting (yellow areas). **f)** Depths to the base of ocean lithosphere (modelled
779 as 1100 and 1200 ˚C isotherms) for ages 0-100 Ma (green lines) and region where mantle residue
780 density increases during melting (light blue area above thin black dashed line). Dark green 1100˚C
781 isotherm from the half-space cooling model (HSM) by Fowler et al., 2005, medium and light green
782 1100 and 1200˚C isotherms by Kawakatsu et al., 2009. Blue arrows indicate downward motion of
783 dense mantle residues, which is in competition with upward ridge suction forces (black arrows).

784

785

786

Figure 3

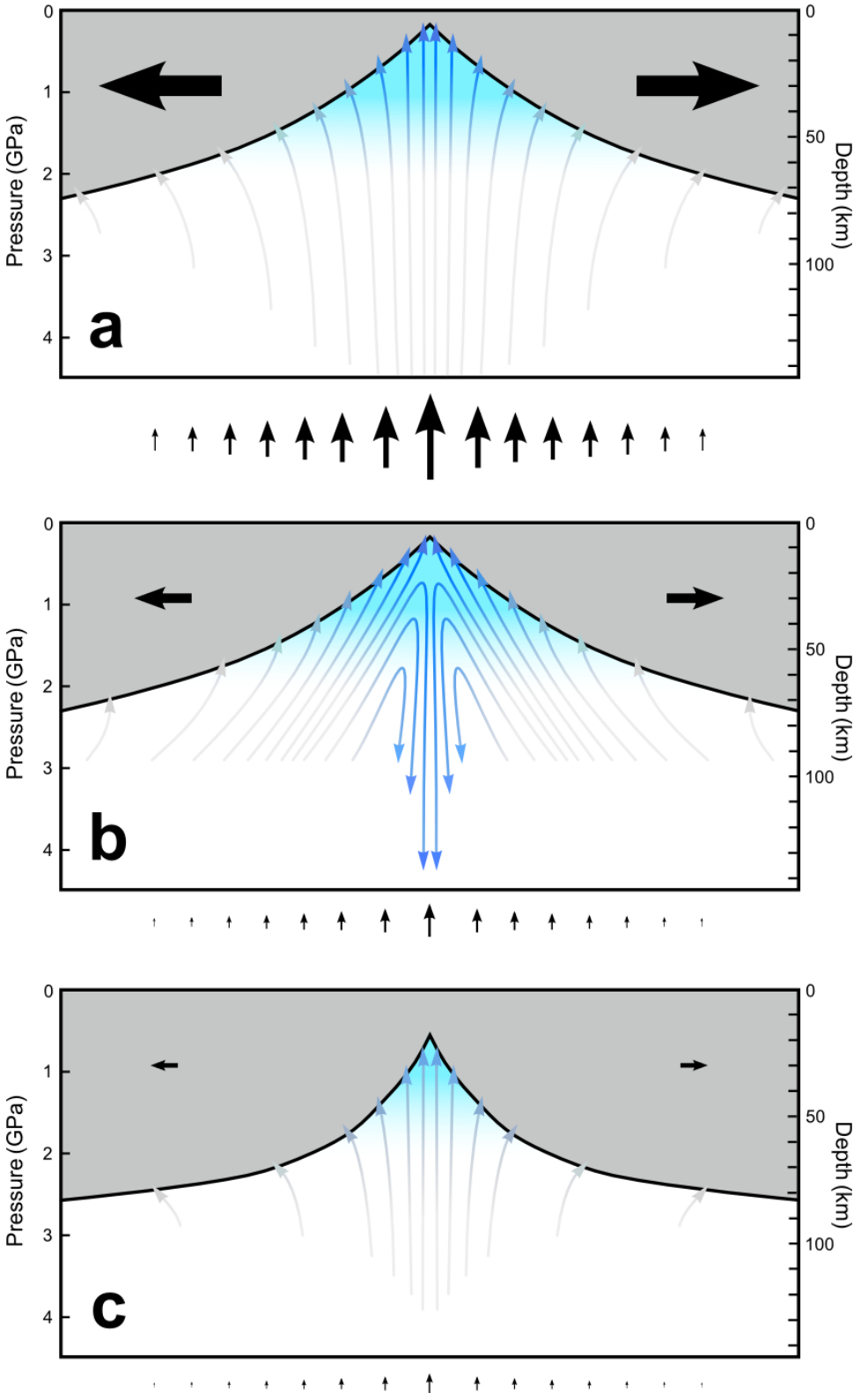

790 **Figure 3.** Schematic model of fast- (a), intermediate-slow (b), and ultra-slow (c) spreading centres and
791 the development of downwellings possibly related to 'hot-spots'. The strength of ridge suction forces
792 that must be overcome by melt residue density increases are indicated beneath each model. Blueness
793 of arrows and asthenosphere indicates degree of partial melting and density increases of mantle
794 residue, respectively. **a)** Fast-spreading centres, where downward density driven forces due to melting
795 are overcome by strong 'ridge suction' forces. Such spreading centres lack 'hot-spots', **b)**
796 intermediate-slow spreading centres, where downward density driven forces locally exceed ridge
797 suction upwelling forces, pulling additional fertile mantle through the melting window. This may result
798 in a melting anomaly, commonly referred to as a 'hot-spot', and **c)** ultra-slow spreading centres, where
799 the general lack of partial melting inhibits the development of downwellings. Such spreading centres
800 lack 'hot-spots'.